HENRY

Hydraulic Engineering Repository

Ein Service der Bundesanstalt für Wasserbau

Conference Paper, Published Version

Souliotis, Dimitris; Prinos, Panayotis

3-D Numerical computations of turbulence in a partially vegetated shallow channel

3-D Numerical computations of turbulence in a partially vegetated shallow channel

D. Souliotis & P. Prinos

Hydraulics Laboratory, Department of Civil Engineering, Aristotle University of Thessaloniki; Thessaloniki, 54006, Greece

ABSTRACT: In the present study three dimensional computations, based on the RANS equations and turbulence models of k-ε and RSM type, have been performed for calculating the flow and turbulence characteristics, such as flow velocity, turbulent kinetic energy, shear stresses and eddy viscosity, in a partially vegetated shallow channel for various vegetation heights and densities, based on laboratory experiments. Computed results are compared with available experimental measurements and expressions from a vortex-based model proposed by the same investigators. In addition, the momentum exchange between the vegetation and the free channel in the lateral direction, and the distribution of flow and turbulence characteristics, mainly at the interface region, are studied.

Keywords: Coherent vortices, Shear stresses, Turbulence models, 3-D computations

1 INTRODUCTION

Open channel shallow flows, partially filled with vegetation, is a problem of increased importance in the last decades which affects many environmental problems such as flow adjacent to terrestrial and aquatic vegetation, discharge capacity of the channels and the mass and momentum exchange between the free flow and the vegetation region which in turn influences the sediment and erosion phenomena.

In the past years several experimental measurements and numerical computations have been performed by various researchers for the study of flow in partially vegetated shallow channels. Ikeda et al. (1991) modeled the sediment transport in a vegetation region using a two-dimensional eddy viscosity model to predict the velocity distribution in the lateral direction of a channel.

More recently Nezu & Onitsuka (2000) measured the turbulence characteristics and observed the development of coherent vortices, due to Kelvin-Helmholtz instability, at the interface region between the vegetation and the free channel flow. The presence of the coherent vortices has been also observed from Large Eddy Simulation (LES) models by Nadaoka & Yagi (1998) and also Xiaohui & Li (2002).

An experimental study has been performed by White & Nepf (2007) for shallow flow in a channel partially obstructed by an array of circular cylinders. They showed that vortices are developed due to the increased shear at the interface and also that the region is divided in two regions. The inner region which establishes the penetration of momentum into the vegetation and the outer region which establishes the scale of the vortices.

Also White & Nepf (2008) proposed a model for the vortex-induced exchange and predicted the distributions of flow velocity and shear stress in shallow channels with a boundary of emergent vegetation. They also found expressions for the penetration length of momentum inside the vegetation and the width of the boundary layer in the main channel.

Several numerical studies on 2D turbulent vegetated flow have been presented recently by various investigators. In these studies the Volume Averaged Reynolds Averaged Navier Stokes (VARANS) equations in conjunction with a turbulence model, based on vegetation dynamics or porous media approach, are employed in order to simulate the effect of vegetation on channel flow and turbulence characteristics.

Li & Yan (2007) used the Spalart-Allmaras model to simulate turbulence while Ayotte et al. (1999) and Choi & Kang (2004) developed Rey-

nolds-stress turbulence models (RSM). Various researchers (Pedras & de Lemos, 2001; Uittenbogaard, 2003; Foudhill et al., 2005 among others) also developed turbulence models of the k-ε type for the same purpose.

In the present study three dimensional computations of the VARANS equations, in conjunction with the k-ε model of Uittenbogaard (2003) and the RSM of Ayotte et al. (1999), which both are based on a vegetation dynamics approach, are used in order to simulate the effect of vegetation on the channel flow. Although the k-ε model cannot simulate the anisotropy of shear stresses, is used in order to be tested on vegetated flows. It is noted that the RSM model is modified (Souliotis & Prinos 2009), for improving the performance of the model. Two cases from White & Nepf (2008) with $C_d\alpha$=9.2 m^{-1} and 28.5 m^{-1} are simulated by the models (C_d = drag coefficient, α = plant density). In addition, numerical computations for two more cases with less dense vegetation ($C_d\alpha = 2$m^{-1} and 5 m^{-1}) have been performed for assessing the effectiveness of the models in a wide range of vegetation densities.

2 GOVERNING EQUATIONS

In this section the VARANS equations are presented together with the transport equations for VA turbulence kinetic energy k, its dissipation ε and the Reynolds stresses $\overline{u_iu_j}$. In the following equations the symbol $<>$ indicates spatial averaged values and for a general parameter ψ the spatial average quantities according to Nikora et al. (2007) are defined as:

$$<\psi> = \frac{1}{A_f}\int_{A_f}\psi\,dA \tag{1}$$

where A_f =volume of fluid contained in the total volume. In the case of spatial–averaged quantities, A_f is parallel to the channel bed and extensive enough to eliminate plant-to-plant variations in vegetation structure but thin enough to preserve the characteristic variation of properties in the vertical.

2.1 VARANS equations

The volume averaged continuity and momentum, equations, according to Raupach & Shaw (1982), Finnigan (2000) and Souliotis & Prinos (2009) are written respectively as:

$$\frac{\partial <U_i>}{\partial x_i} = 0 \tag{2}$$

$$<U_j>\frac{\partial <U_i>}{\partial x_j} = -\frac{1}{\rho}\frac{\partial <P>}{\partial x_j} + \frac{\partial}{\partial x_j}<-\overline{u_iu_j}>$$
$$-\frac{\partial}{\partial x_j}<\tilde{U}_i\tilde{U}_j> -0.5C_d\alpha|U|<U_i> \tag{3}$$

where U_i = fluid velocity in the x_i direction, ρ = fluid density, P = effective pressure, $\overline{u_iu_j}$ = Reynolds stresses,. The third term in the rhs of Eq. (3) is an "additional dispersive" term, due to correlation of spatial deviations of the mean velocity components, which can be assumed negligible in flows with high density. The last term in Eq. (3) is an extra drag term due to vegetation resistance.

The Reynolds stresses,$<-\overline{u_iu_j}>$, are calculated through the Boussinesq hypothesis for the $<k>$-$<\varepsilon>$ model as follows:

$$<-\overline{u_iu_j}>=<v_t>\left(\frac{\partial <U_i>}{\partial x_j}+\frac{\partial <U_j>}{\partial x_i}\right)-\frac{2}{3}<k>\delta_{ij} \tag{4}$$

where v_t= turbulent viscosity ($= C_\mu<k>^2/<\varepsilon>$, $C_\mu = 0.09$) and δ_{ij} = Kronecker delta.

2.2 Transport equations for $<k>$, $<\varepsilon>$ and $<\overline{u_iu_j}>$

The transport equation for the turbulent kinetic energy, $<k>$ and the dissipation rate $<\varepsilon>$ are derived from the VA (Volume Average) of the original transport equations for k and ε. For the $<k>$-$<\varepsilon>$ model the equation for $<k>$ is:

$$<U_j>\frac{\partial <k>}{\partial x_j} = \frac{\partial}{\partial x_j}\left(\frac{<v_t>}{\sigma_\kappa}\frac{\partial <k>}{\partial x_j}\right)$$
$$+ <-\overline{u_iu_j}>\frac{\partial <U_i>}{\partial x_j} - <\varepsilon> +0.5C_d\alpha|U|<U>^2 \tag{5}$$

The last term is an additional source term due to vegetation while the additional dispersive terms resulting from the volume averaging of the convection and the diffusion terms are assumed negligible. For the RSM model the turbulence kinetic energy $<k>$ is not computed through a transport equation since it is obtained directly from the normal Reynolds stresses ($<k>=0.5<\overline{u_iu_i}>$).

For the $<k>$-$<\varepsilon>$ (Uittenbogaard, 2003) and the RSM models the respective equations for $<\varepsilon>$ are written in a similar way to the $<k>$ equation and they take the respective forms:

$$<U_j>\frac{\partial <\varepsilon>}{\partial x_j} = \frac{\partial}{\partial x_j}\left(\frac{<v_t>}{\sigma_\varepsilon}\frac{\partial <\varepsilon>}{\partial x_j}\right) - c_{\varepsilon 2}\frac{<\varepsilon>^2}{<k>}$$
$$+c_{\varepsilon 1}\frac{<\varepsilon>}{<k>}\times<-\overline{u_iu_j}>\frac{\partial <U_i>}{\partial x_j} + 0.5C_d\alpha c_{\varepsilon 2}\left(t_{eff}^{-1}\right)|U|<U>^2 \tag{6}$$

$$<U_k> \frac{\partial <\varepsilon>}{\partial x_j} = c_\varepsilon \frac{\partial}{\partial x_k} \left(\frac{<k>}{<\varepsilon>} <\overline{u_k u_l}> \frac{\partial <\varepsilon>}{\partial x_l} \right)$$

$$+ c_{\varepsilon l} \frac{<\varepsilon>}{<k>} <\overline{-u_i u_k}> \frac{\partial <U_i>}{\partial x_k} - c_{\varepsilon 2} \frac{<\varepsilon>^2}{<k>} + 0.5 t_{eff}^{-1} d_{ii}$$

(7)

where σ_κ, σ_ε = constants (= 1.0, 1.3 respectively), $c_{\varepsilon l}$, $c_{\varepsilon 2}$ = constants (=1.51, 1.92 for the $<k>$-$<\varepsilon>$ model and =1.44, 1.92 for the RSM model), t_{eff} = time scale variable, based on geometrical and turbulence characteristics (Uittenbogaard, 2003) and $<d_{ij}>$ = foliage contribution associated with work against pressure and viscous drag on the vegetation (Ayotte et al., 1999). The last terms in Eq. (6) and (7) are additional production terms of dissipation ε due to vegetation. The $<\varepsilon>$-equation, for the RSM model of Ayotte et al. (1999) has been modified and a more detailed analysis of the modified approach can be found in Souliotis & Prinos (2009).

The RSM model calculates the Reynolds stresses $<\overline{u_i u_j}>$ using a transport equation which takes the following form:

$$<U_k> \frac{\partial <\overline{u_i u_j}>}{\partial x_k} = \frac{\partial}{\partial x_k} \left(\frac{<v_t>}{\sigma_\kappa} \frac{\partial <\overline{u_i u_j}>}{\partial x_k} \right)$$

$$+ \left(<\overline{-u_i u_k}> \frac{\partial <U_j>}{\partial x_k} + <\overline{-u_j u_k}> \frac{\partial <U_i>}{\partial x_k} \right)$$

(8)

$$+ <\varphi_{ij}> - \frac{2}{3} \delta_{ij} <\varepsilon> + \frac{1}{3} 0.5 C_d \alpha |<U>|^3$$

where φ_{ij}=pressure strain term (FLUENT INC., 2001). The last term in Eq. (8) is an extra term due to the vegetation and is only used in the transport equations for the normal stresses.

3 NUMERICAL PROCEDURE - CASES STUDIED

The FLUENT 6.0.12 CFD code, based on a finite volume technique, is used for the numerical computations. The code solves Eqns. (2), (3), (5), and (6) when the $<k>$-$<\varepsilon>$ model is applied while Eq. (2), (3), (7) and (8) are solved when the RSM model is used. The extra source terms, due to the presence of vegetation are introduced in the above equations, using User Defined Functions (UDF) which are based on a C code.

For the grid construction the GAMBIT program was used. The grid was three-dimensional, structured and the shape of the cells was orthogonal. Several runs with different number of computational cells showed that the numerical results are grid independent. In the present work the grid size is equal to 5x240x20 (streamwise, lateral, and vertical direction respectively). The grid density is

increased near the walls and also at the interface region (vegetation-free channel) due to the increased shear.

At the entrance and the exit of the flow periodic conditions were used in order to avoid the increased length which is needed for the flow to become fully developed. For the free surface, symmetry boundary conditions were used. In Figure 1 a three dimensional view of the vegetated and the free channel regions is shown.
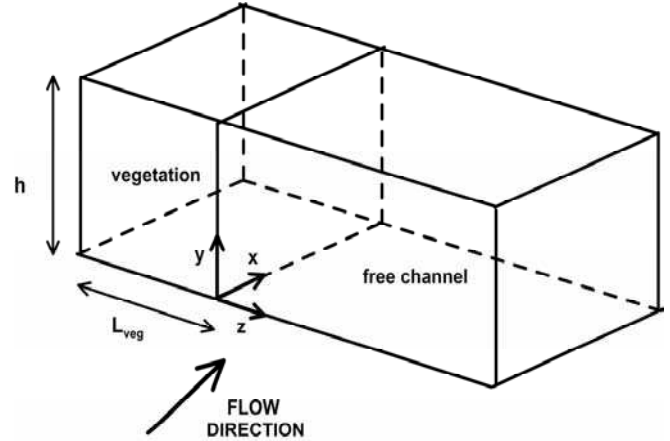

Figure 1: 3-D view of the total channel region

Experimental measurements from White & Nepf (2008) are used for the evaluation of the turbulence models. In these experiments a 1.2m wide and 13m long flume partially filled with a 0.4m wide array of cylinders, with 0.0065m diameter, which simulates the vegetation, were used. The flow depth was varied between 0.066m and 0.068m while the channel slope S_o was 2.29×10^{-4}. The porosity of the modelled vegetation varied between a minimum value of 0.9 and a maximum of 0.98 which corresponds to $C_d \alpha = 274$ m^{-1} and 9.2 m^{-1} respectively. In the present paper two cases from White & Nepf (2008) with $C_d \alpha = 9.2$ m^{-1} and 28.5 m^{-1} are used. In addition, numerical computations for two more cases with less dense vegetation ($C_d \alpha = 2$ m^{-1} and 5 m^{-1}) have been performed.

4 ANALYSIS OF RESULTS

Initially the variation of fully developed local mean velocities $<U>$ and shear stress $<-uw>$, computed by both models, within the cross-section is presented for $C_d \alpha$=9.2 m^{-1}.

Figure 2 shows the contours of streamwise velocity, made dimensionless with the maximum local velocity at the free channel flow (U_{max}). Inside the vegetation low values are observed for both models. At the free channel region higher values are observed at the center of the channel and near the free surface. According to the $<k>$-$<\varepsilon>$ model the distribution of flow velocity is more uniform

in the central part of the free channel, in contrast to the RSM model, which shows that at the channel corner a bulging of the contours occurs due to the secondary currents predicted by the model in the corner region.
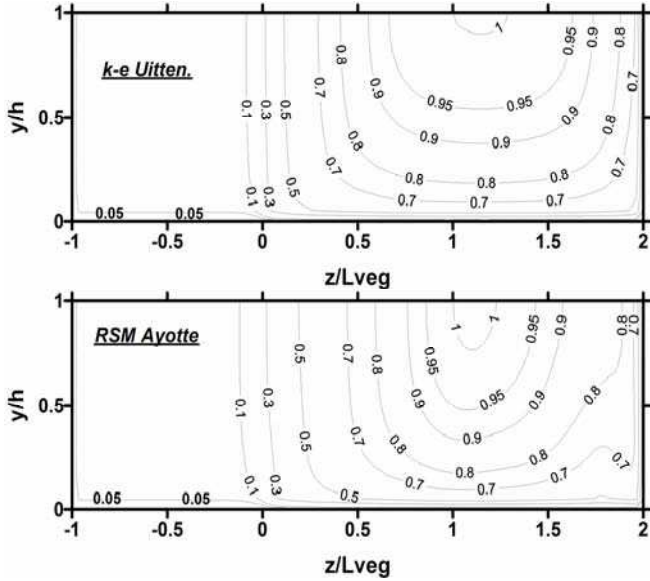

Figure 2: Contours of dimensionless streamwise velocity $<U>/U_{max}$ for $C_d\alpha = 9.2$ m^{-1}.

In Figure 3 the contours of local shear stress ($<-uw>$) are shown. The local shear stress has been made dimensionless with the depth-averaged shear stress at the interface ($<-\overline{uw}>_{int}$). At the interface region and for $y/h>0.5$ higher values of $<-uw>$ are observed due to increased velocity gradients in the lateral direction. Inside the vegetation shear stresses have very low values which mean that the presence of vegetation damps the turbulence within the vegetation and flow may become laminar. At the centre of the channel, the effect of the side wall and the interface region is reduced, and the values of $<-\overline{uw}>$ are reduced as it is expected.
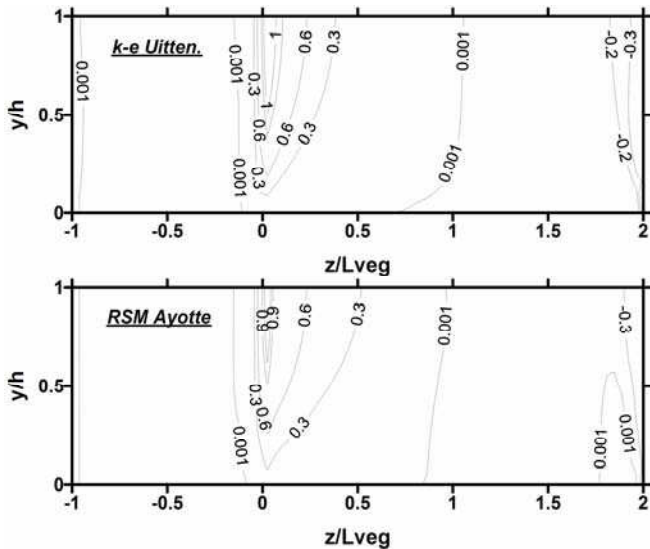

Figure 3: Contours of dimensionless shear stress $<-\overline{uw}>/<-\overline{uw}>_{int}$ for $C_d\alpha = 9.2$ m^{-1}.

In the following paragraphs the distributions of depth-averaged mean velocity and turbulence characteristics (turbulence kinetic energy, Reynolds stresses and turbulent viscosity) are presented and compared with available experimental data and empirical relations from White and Nepf (2008). For the sake of brevity the subscript denoting depth-averaged values has been removed from all parameters.

In Figure 4 the distributions of wall (bed, sidewalls) shear stresses as well as the depth-averaged shear stress $\rho<-\overline{uw}>$ are shown. They have been made dimensionless with γhS_o, ($\gamma = \rho g$). For both cases the stresses at the side wall of the free channel are higher in comparison to those at the side wall adjacent to the vegetation, due to the high flow velocity in the free channel. The RSM model provides higher values at the free channel side wall. The bed shear stress in the vegetation region has low values due to the reduced flow velocity, while in the free region, where the distribution of τ_{bed} also follows the development of flow velocity, increased τ_{bed} values occur at the central part of the channel. The RSM model presents increased τ_{bed} values near the corner region, due the capability of the model to compute the secondary currents generated by the anisotropy of the normal stresses.
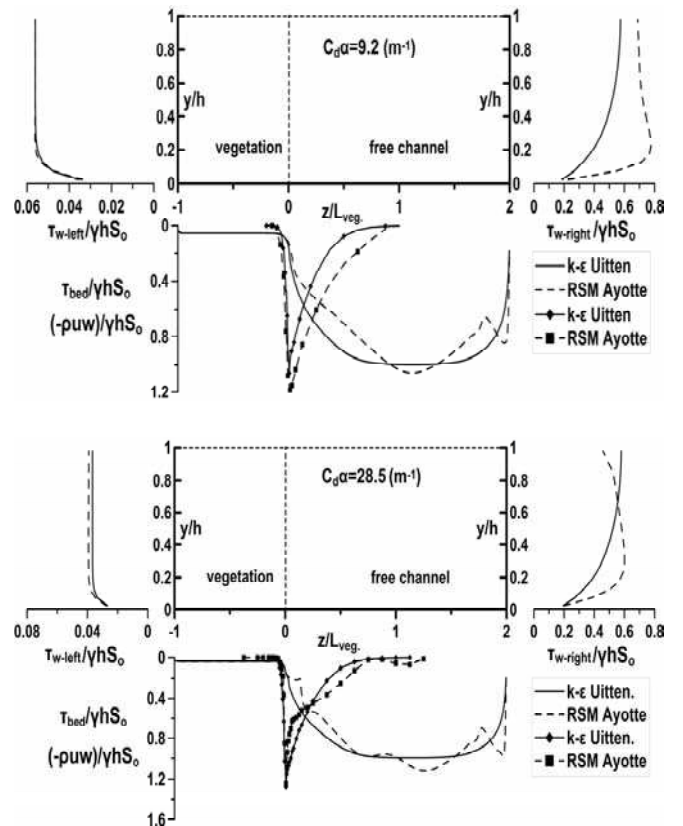

Figure 4. Distribution of wall shear stress τ_{wall} and depth-averaged shear stress $\rho<-\overline{uw}>$.

Figure 5 reveals the contribution of free channel bed shear stress (τ_{bed}), wall shear stress at the side wall of the free channel (τ_{wall}) and the shear

86

stress at the interface ($\tau_{int.}$), made dimensionless with the total free channel stress ($\tau_{tot.} = \tau_{bed} + \tau_{wall} + \tau_{int}$). In order to get a more clear view, results from two more cases, with $C_d\alpha = 2$ and 5 m^{-1}, are used. As it is shown τ_{bed} has dominant role (86-90% of the total stresses), while the effect of the interface and the side wall is lower, with a varied contribution of 6-10% and 4-4.5% respectively. The increased values at the interface region in comparison to those at the side wall can be attributed to the momentum exchange between free channel and vegetation flows.
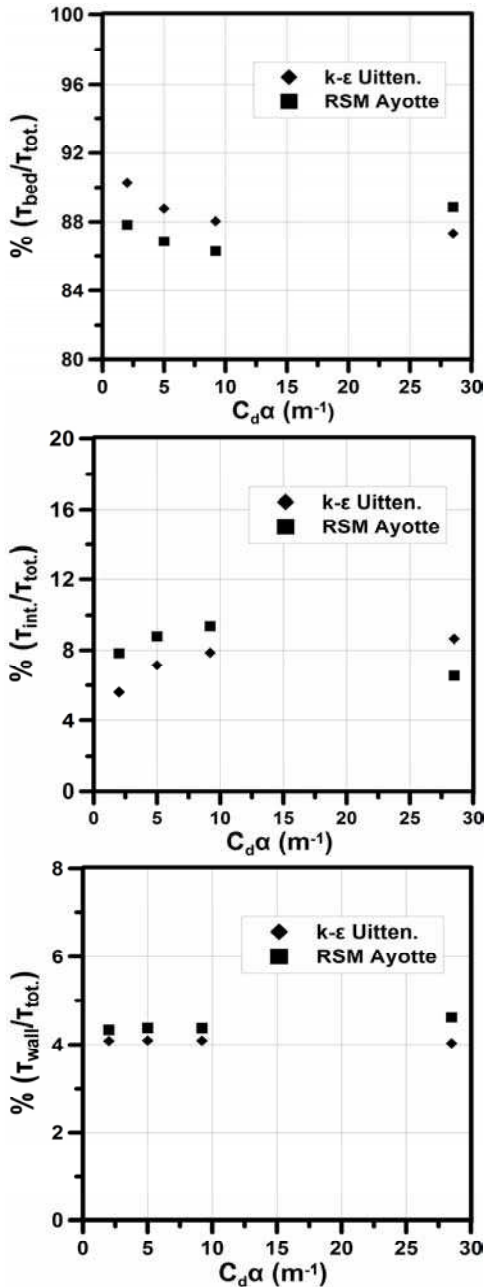

Figure 5. Wall and interfacial stresses contributions to total free channel stress for various vegetation densities.

The $\langle k \rangle$-$\langle \varepsilon \rangle$ Uittenbogaard (2003) model provides higher values for τ_{bed} in comparison to the RSM model while the respective values for τ_{wall} and $\tau_{int.}$ are lower. However, this behavior is not observed for the high density case.

In Figure 6 the variation of depth-averaged streamwise velocity, made dimensionless with the maximum depth averaged velocity at the free channel flow (U_2), in the lateral direction is shown, for both turbulence models. Inside the vegetated region the flow velocity is uniform and the computed results coincide with the experimental measurements. The momentum equation, inside the vegetation is simplified to a balance between the drag and the bed gradient. At the interface region an inflection point is observed due to the momentum exchange and the associated increased shear due to the difference of flow velocity between free channel and the vegetated area. Shear layer type profiles are developed at the free channel region and, according to the $\langle k \rangle$-$\langle \varepsilon \rangle$ Uittenbogaard (2003) model, the flow becomes uniform in a wider central area in comparison to that of the RSM model. The experimental measurements are in agreement with the RSM results and as it is expected the region of uniform flow velocity is increased for the sparser case ($C_d\alpha = 9.2$ m^{-1}). The effect of the side channel wall is significant for $z/L_{veg.} > 1.25$ according to the RSM model, while the respective region according to the $\langle k \rangle$-$\langle \varepsilon \rangle$ model is decreased ($z/L_{veg.} > 1.6$).
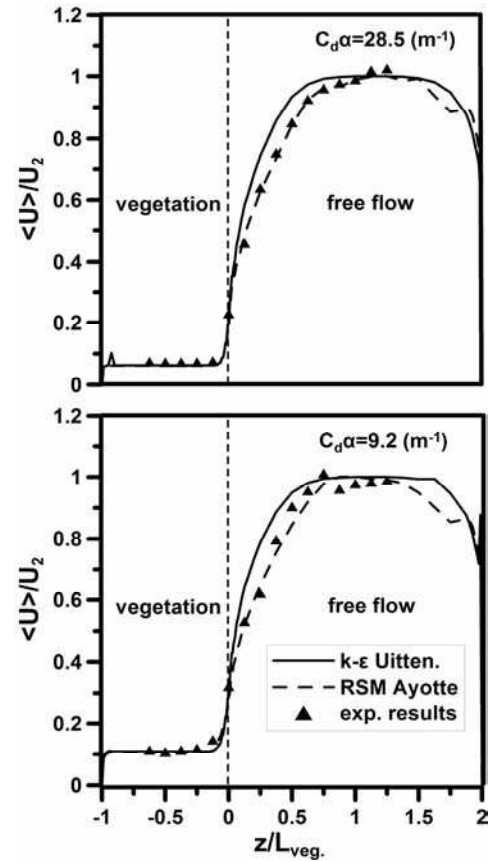

Figure 6. Computed and experimental streamwise, depth-averaged velocity distributions.

In Figure 7 the distribution of the depth-averaged shear stress ($\langle -\overline{uw} \rangle$) is shown. The shear stress has been made dimensionless with the square of friction velocity at the interface U_*^2

(=max$(<-\overline{uw}>)$). The profiles demonstrate that maximum values occur at the interface. Inside the vegetation $<-\overline{uw}>$ is reduced rapidly, while in the free channel the respective decrease is more gradual. The two turbulence models reveal identical behavior in the vegetation region, while in the free flow the values of $<-\overline{uw}>$ according to the $<k>-<\varepsilon>$ Uittenbogaard (2003) decrease more rapidly in comparison to those of the RSM Ayotte et al. (1999) model. In this region the experimental measurements are in agreement with the RSM model for both cases while at the interface the maximum values are higher in comparison with the computed results. This means that shear at the interface is higher and hence the length in which high momentum fluid penetrates inside the vegetation is increased as it is shown for the sparse case ($C_d\alpha = 9.2$ m^{-1}). The higher value of experimental shear stresses, for the denser case, has negligible effect on the penetration of high momentum fluid, which means that the increased vegetation density has dominant role.
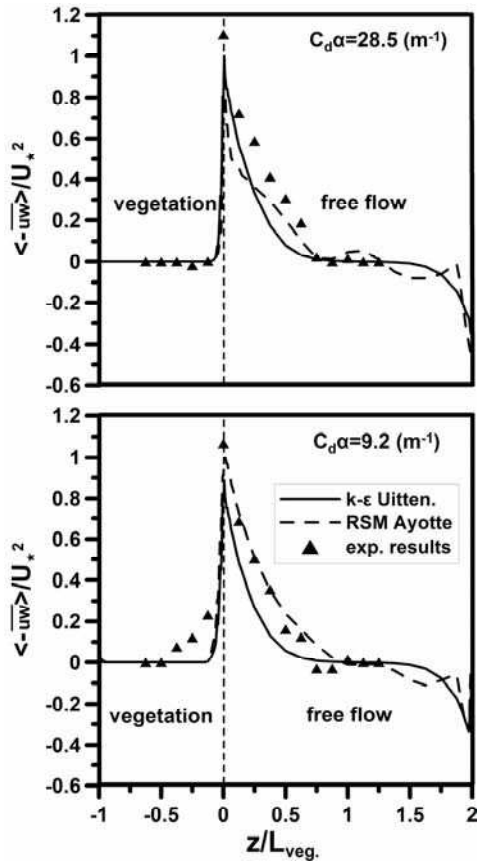

Figure 7. Distributions of computed and experimental depth-averaged shear stress $<-\overline{uw}>$.

Similar results are observed from Figure 8 where dimensionless (with U_*^2) distributions of turbulent kinetic energy are shown. Inside the vegetation the RSM model computes negligible values in comparison to those of the $<k>-<\varepsilon>$ model, which is caused due to an extra source term in $<k>$ equation which simulates the presence of vegetation. For the $<k>$ there are no available experimental measurements for comparison with the computed results. The above results are in agreement with White & Nepf (2007) who have shown that two distinct regions exist in the shear layer. The region, called inner layer, where momentum can penetrate into the vegetation with length δ_I and the region (outer layer) outside the vegetation, with length δ_O, where boundary layer profiles are developed. The δ_I is taken as the distance from the interface to the point where Reynolds stresses decays to 10% of its maximum value (Nepf et al., 2007) while δ_O is taken as the distance from the interface to the point where flow velocity reaches its uniform value in the free channel. The distance δ_I can be computed with high accuracy since the number of the grid points is increased in this region and hence the error is negligible.
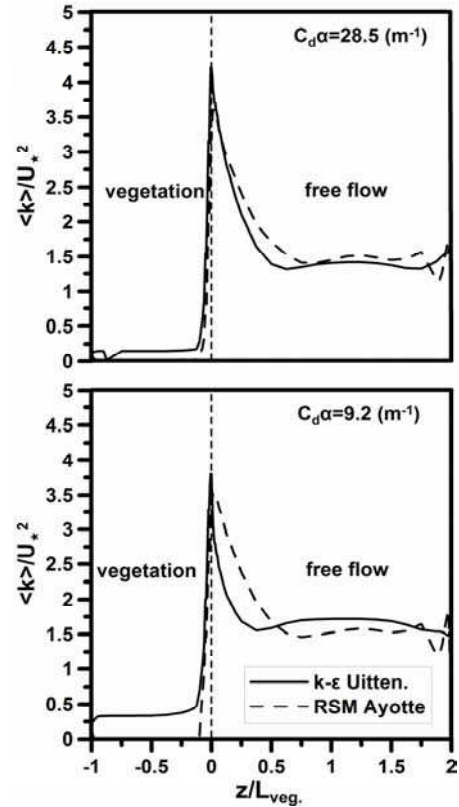

Figure 8. Computed distribution of turbulent kinetic energy.

In Figure 9 the inner layer profiles are shown and are compared to an hyperbolic profile presented by White & Nepf (2008):

$$\frac{U-U_I}{U_s} = \left[1 + \tanh\left(\frac{z-z_o}{\delta_I}\right)\right] \quad (9)$$

where U_I = the depth-averaged uniform velocity inside the vegetation, z_o = the inflection point (which coincides with the interface) and U_s = the depth averaged slip velocity, equal to U_{zo} - U_I. The computed normalized velocity profiles and the hyperbolic profile are in agreement at the in-

88

terface, however in the inner layer the comparison is less satisfactory. Inside the vegetation region the profiles from the turbulence models and from Eq. (9) coincide.
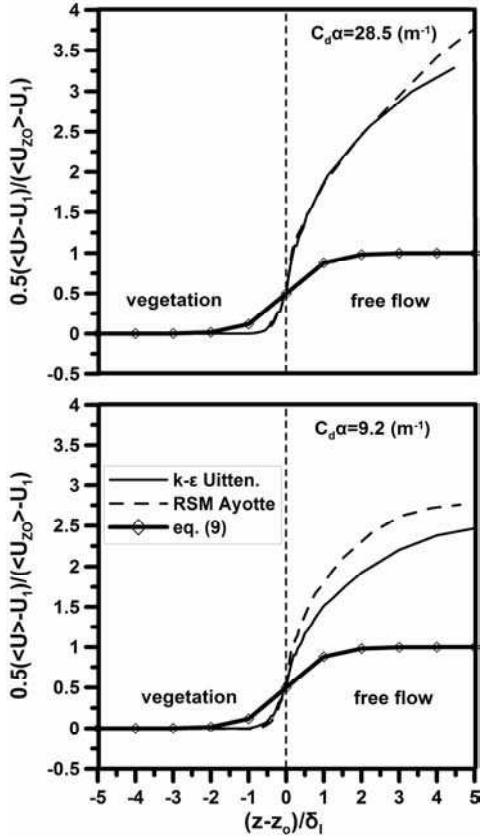

Figure 9. Normalized inner layer profile.

Outside the vegetation the hyperbolic profile fails to follow the computed profiles. For this region the computed outer layer profiles are compared (Figure 10), to a parabolic velocity profile presented by White & Nepf (2008):

$$\frac{U - U_m}{U_2 - U_m} = \left[\frac{z - z_o}{\delta_O} - \frac{1}{4}\left(\frac{z - z_m}{\delta_O}\right)^2\right] \tag{10}$$

where z_m = the point at which the inner and the outer layer slope match and U_m = the velocity at z_m. In the present work $z_m = 0$ (coincides with the interface) and U_m is equal to the velocity at the interface. The comparison shows that the computed velocities from the turbulence models are developed more rapidly and reach uniform values, at the free channel, earlier than those computed by the parabolic profile.

In Figure 11 the profiles of normalized eddy viscosity for the two cases are shown. The eddy viscosity has the higher values for both models at the free channel region ($z/\delta_O = 0.2$) where the coherent vortices, due to the shear at the interface, are increased. Inside the vegetation v_t decreases rapidly and for $z/\delta_O < -0.2$ has negligible values which means that the vortices are unable to penetrate deeper, due to the increased vegetation densi-

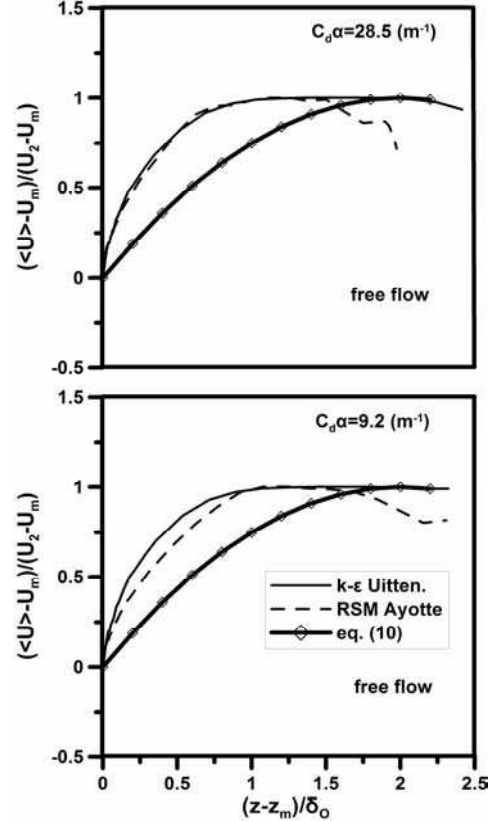ty. Both models demonstrate similar behavior for the two cases.
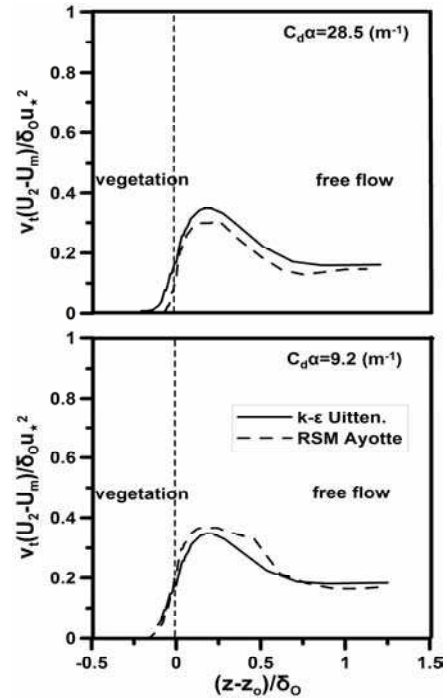

Figure 10. Rescaled outer layer profiles.

Figure 11. Distributions of normalized eddy viscosity.

5 CONCLUSIONS

In the present study flow and turbulence characteristics have been computed for a three- dimensional partially vegetated shallow flow. Distributions of flow velocity, shear stresses and turbulent

89

kinetic energy, in the lateral direction, show that at the interface region increased shear is observed due to the momentum exchange and the interaction between the vegetation and the free channel flow.

The produced coherent vortices penetrate into vegetation and this penetration length decreases with density while in the outer region the effect of vegetation density is negligible and boundary profiles of flow velocity are developed. Inside the vegetation where the coherent vortices are unable to penetrate the flow is uniform and the computed values for shear stresses ($<-\overline{uw}>$) and turbulent kinetic energy ($<k>$) are very low. At the central part of the free channel, where the effect of vegetation is also decreased, reduced variations of flow and turbulence characteristics are observed, with the $<k>$-$<\varepsilon>$ Uittenbogaard (2003) model to provide wider areas of constant values. However the modified RSM model demonstrates in general better behavior when its numerical results are compared with experimental measurements for $<U>$ and $<-\overline{uw}>$. As it is also shown the channel bed provides the higher contribution to the total wall shear stress and also the wall stress, at the corner region, demonstrates increased variation in comparison to that of the $<k>$-$<\varepsilon>$ model due to the capability of the RSM model to predict secondary currents correctly.

REFERENCES

Ayotte, K.W., Finnigan, J.F., Raupach, M.R. 1999. A second-order closure for neutrally stratified vegetative canopy flow. Boundary Layer Meteorology, 90, 189-216.

Choi, S. U., Kang, H. S. 2004. Reynolds stress modelling of vegetated open-channel flows. Journal of Hydraulic Research, IAHR, 42(1), 3-11.

Finnigan, J., 2000. Turbulence in plant canopies. Annual Review of Fluid Mechanics, 32, 519-571.

FLUENT INC. 2001. Fluent 6.0 Documentation. Lebanon, USA.

Foudhill, H., Brunet, Y., Caltagirone, J-P. 2005. A fine-scale k-ε model for atmospheric flow over heterogeneous landscapes. Environmental Fluid Mechanics, 5, 247-265.

Ikeda, S., Izumi, N., Ito, R. 1991. Effects of pile dikes on flow retardation and sediment transport. Journal of Hydraulic Engineering, ASCE, 117(11),1459-1478.

Li, C. W., Yan, K., 2007. Numerical investigation of wave-current-vegetation interaction. Journal of Hydraulic Engineering, ASCE, 133(7), 794-803.

Nadaoka, K., Yagi, H. 1998. Shallow-water turbulence modelling and horizontal large-eddy computation of river flow. Journal of Hydraulic Engineering, ASCE, 124(5), 493-500.

Nezu, I., Onitsuka, K. 2000. Turbulent structures in partially vegetated open-channel flows with LDA and PIV measurements. Journal of Hydraulic Research, IAHR, 39(6), 629-642.

Nepf, H., Ghisalberti, M., White, B., Murphy, E., 2007. Retention time and dispersion associated with submerged aquatic canopies. Water Resources Research, 43, W04422, doi:10.1029/2006WR005362.

Nikora, V.I., McEwan, I.K., McLean, S.R., Coleman, S.E., Pokrajac, D., Walters, R. 2007. Double-Averaging Concept for Rough-Bed Open-Channel and Overland Flows: Theoretical background. Journal of Hydraulic Engineering, ASCE,, 133,873-883.

Pedras M.H.J., de Lemos M.J.S. 2001. Macroscopic turbulence modelling for incompressible flow through undeformable porous media. International Journal of Heat and Mass Transfer, 44, 1081-1093.

Raupach, M.R., Shaw, R.H. 1982. Averaging procedures for flow within vegetation canopies. Boundary Layer Meteorology, 22, 79-90.

Souliotis, D., Prinos, P. 2009. Macroscopic turbulence models and their application in turbulent vegetated flows, Journal of Hydraulic Engineering, ASCE, (under review).

White, B., Nepf, H. 2007. Shear instability and coherent structures in shallow flow adjacent to a porous layer. Journal of Fluid Mechanics, 593, 1-32; DOI:10.1017/S0022112007008415.

White, B., and Nepf, H. 2008. A vortex-based model of velocity and shear stress in a partially vegetated shallow channel. Water Resources Research, 44, W01412; DOI: 10.1029/2006WR005651.

Uittenbogaard R. 2003. Modelling turbulence in vegetated aquatic flows. Riparian Forest Vegetated Channels Workshop, Trendo, Italy.

Xiaohui, S., Li, C. 2002. Large eddy simulation of free surface turbulent flow in partly vegetated open channels, International Journal for Numerical Methods in Fluids, 39, 919-937.